Performance and Efficiency Mapping of Externally Excited Synchronous Machines

Performance and Efficiency Mapping of Externally Excited Synchronous Machines

Andreas Carlsson
Electric Drive Unit – CAE & EMD
Polestar Performance AB
Gothenburg, Sweden
Andreas.Carlsson@Polestar.com

Felix Andersson
Electric Drive Unit – CAE & EMD
Polestar Performance AB
Gothenburg, Sweden
Felix.Andersson@Polestar.com

Irene Santantonio
Electric Drive Unit – CAE & EMD
Polestar Performance AB
Gothenburg, Sweden
Irene.Santantonio@Polestar.com

Viktor Josefsson
Electric Drive Unit – CAE & EMD
Polestar Performance AB
Gothenburg, Sweden
Viktor.Josefsson@Polestar.com

Gabriele Puccio
Electric Drive Unit – CAE & EMD
Polestar Performance AB
Gothenburg, Sweden
Gabriele.Puccio@Polestar.com

Sandro Rubino
Dipartimento Energia "G. Ferraris"
Politecnico di Torino
Torino, Italy
sandro.rubino@polito.it

***Abstract* – This paper presents the process of analyzing the performance of an externally excited synchronous machine (EESM). The paper aims to provide engineers and researchers with a simple process to extract motor maps using finite element analysis (FEA) followed by an analytical post-processing of the simulation results. An example motor is considered where the flux maps are extracted through FEA calculations and then used to define the operational limits of the motor at a specific dc-link voltage level using an optimization algorithm. Within the operational limits of the motor, the losses are then minimized and finally, the results from the optimization are shown.**

Keywords—Traction Motor, Externally Excited Synchronous Machines, Efficiency Map, Maximum Torque Per Loss

I. INTRODUCTION

As the automotive sector moves towards more sustainable solutions with a large focus on electrification, different electrical machine types have been investigated. Permanent magnets synchronous machines (PMSM) represent the most commonly used topology due to their high torque and power density combined with a high efficiency [1]. However, these kinds of machines also come with a number of disadvantages, such as the utilization of rare earth elements in the permanent magnets, where significant research has been done to reduce their volume [2-3]. In addition, the rotor magnetic field leads to high no load losses in the stator iron in the form of eddy currents as the rotor is rotating.

Other machine types that may be used for automotive applications are induction machines (IM) and synchronous reluctance machines (SRM) but both come with the downside of reduced efficiency and lower torque density [4]. Therefore, from a performance perspective, these motors are less attractive for traction application.

One more machine type has recently become a viable option for automotive applications: the externally excited synchronous machine (EESM).

Maintaining similar performances compared to PMSMs, EESMs are characterized by the rotor field generated through an electromagnet instead of the utilization of permanent magnets [5]. The use of an electromagnet not only removes the need for rare earth elements but also enables the opportunity to control the magnetic field produced by the rotor actively [5-6]. This enables one more degree of optimization of the machine control, which enables EESMs to achieve higher power at high speed and different efficiency profiles as compared to conventional PMSMs [7]. In addition, the EESM is more fault tolerant than the PMSM since the permanent magnets can cause significant short circuit currents in the windings as well as uncontrolled generator operation [8] to the battery at high speed. Because of the control of the field current, the two above issues can be mitigated, and therefore, the EESM requires fewer safety measures [9].

Another advantage of the EESM is that the rotor can safely operate at higher temperatures compared to most common PMSMs for automotive applications. This is due to the rotor insulation system, which can be designed to handle temperatures up to 180 °C if using an H-class insulation system. Permanent magnets often used for automotive applications are SH- or UH-grade, where, for high-power applications, the UH-grade can safely operate to up to 150 °C whilst minimizing the risk of demagnetization under fault conditions. In some cases, EH-grade magnets can be used to increase the temperature at which the PMSM can operate safely. However, EH-grade magnets imply an increased use of rare earth elements, specifically dysprosium, leading to a significantly higher unit cost.

When designing electrical machines for traction applications, efficiency maps, which display the overall efficiency during different load cases, represent one of the tools used for analyzing motors. There are several methods which can be used to obtain efficiency maps. Typically, these methods are based on FEA or actual test data. One of the most important aspects when obtaining the efficiency map is the strategy used to determine the operating conditions at each operation point. The most implemented strategy typically is the maximum torque per ampere (MTPA) which can be applied easily to most types of electrical machines [10]. However, for EESM, an MTPA-based strategy is not suggested since it leads to the maximization of the rotor current, i.e., the rotor Joule losses. Therefore, other methods must be used. Control strategies like copper loss minimization [6] or maximum torque per loss (MTPL) are among these methods.

According to this scenario, this paper proposes a method to accurately evaluate performance profiles and efficiency maps of EESMs by using a combination of FEA and analytical calculations.

The paper is organized as follows. Section II describes general principles regarding the EESM, while the motor used as the case of study is described in Sector III. Section IV presents the method to obtain the flux maps, and general recommendations for modelling and data resolution are provided. In Section V, the mathematical modeling of the EESM and proposed calculation method to compute the performance profiles of the motor are described, and results obtained from the case study are shown. Finally, conclusions are given in section VI.

II. EXTERNALLY EXCITED SYNCHRONOUS MACHINES

The EESM is similar to the PMSM in its general physics but possesses some key differences. EESM utilizes rotor windings to generate the electromagnetic field in the rotor by applying an external dc current. The rotor field interacts with the stator field created by the stator winding to produce torque. The external rotor supply introduces an additional degree of freedom, allowing the direct control of the field current and providing a more precise regulation of the flux level toward more efficient operation areas of the electrical machine, specifically at low torque and higher speed. In EESMs, the possibility to adjust the level of rotor flux enables a reduction in the contribution of the iron losses in the stator steel lamination, while, in PMSMs, due to the constant level of the flux generated by permanent magnets, the high level of the iron losses in the lamination is kept even at low torque operating regions [6-7].

In addition, the control of the rotor field results in a motor that is able to deliver a high level of torque at high speed, which leads to higher output power when compared to the traditional PMSM and allows for a significantly higher power factor. These attributes make EESM topology an attractive option for the automotive industry since both improved efficiencies and performances can be achieved in the region where vehicles often operate, and the use of rare earth elements is completely eliminated.

One of the main challenges with EESMs is the rotor excitation system, for which two leading solutions are being developed. The first uses conventional brushes, but such a solution brings shortcomings like additional mechanical friction losses and possible reliability issues through additional wear. The second solution is using rotating transformers fed by an external H-bridge converter. This solution is more complex than the brushed system and poses control and thermal management challenges. Another challenge is the manufacturing of the rotor itself where the utilization of concentrated winding in combination with a high number of field turns causes long production times and hence forcing multiple parallel production lines which drives up cost. Typically needle winding is utilized and one of the main disadvantages with this is that the copper fill factor in the slots will be lower as there must be sufficient space within the slot to fit the needle between the coils.

III. MOTOR STUDIED

The motor under study is an 8-poles, 48-slots EESM designed to deliver 450 Nm at a maximum current of 450 Arms. The peak power at 700 Vdc is 300 kW. The primary specifications of the motor are reported in Table I. Fig. 1 shows the rotor and the stator cross-section of the designed motor.

TABLE I. MOTOR PERFORMANCE AND GEOMETRY PARAMETERS.

Motor design parameter	Unit	Value
Peak Power	kW	300
Maximum torque	Nm	450
Maximum current	Arms	450
Maximum Voltage	V	700
Stator outer diameter	mm	200
Stator inner diameter	mm	127.5
Active length	mm	125
Slot number	-	48
Pole number	-	8
Number of phases	-	3

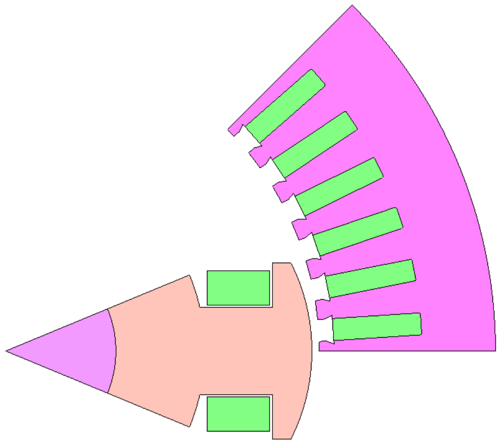

Fig. 1. The studied motor topology and outline.

IV. EESM FLUX MAPS

A. Simulation Methodology

The flux maps of the motor are obtained through FEA, in which the stator *dq* currents and rotor field current are imposed for a range of speeds from zero up to the maximum operative limit of the machine. In detail, for each speed, several combinations of stator *dq* currents and rotor field current are imposed according to a regular 3D mesh grid. Simulating at different speeds allows for accurate calculation of the eddy current effects on the output torque. In addition to the flux maps, total losses and losses per component are extracted to solve the MTPL algorithm.

The adopted FEA model is significantly simplified to speed up the calculation of the flux maps where a pure sinusoidal current excitation for the stator and a pure dc current source in the rotor are used. The simulation time is set to one electric cycle, in turn subdivided into 60 steps. This low number of steps per cycle results in a reduction in accuracy when calculating the torque ripple. However, it is sufficient to calculate the fundamental parameters required to obtain the flux maps, such as the average value per cycle of electromagnetic torque T, stator copper losses P_{Cu}, iron losses P_{Iron_Loss}, and stator dq flux linkages (ψ_d,ψ_q).

TABLE II. COMPARISON BETWEEN 60 STEPS PER CYCLE AND 120 STEPS PER CYCLE.

Variable	60 Steps	120 Steps	Difference [%]
T [Nm]	203.2	203.1	0.05
ψ_d [Wb]	0.00302	0.00306	-1.3
ψ_q [Wb]	0.02137	0.02155	-0.84
T_{ripple} [%]	12.91 %	13.63 %	-5.28
P_{Iron_Loss} [kW]	1.479	1.500	-1.4
P_{Cu} [kW]	11.589	11.750	-1.37

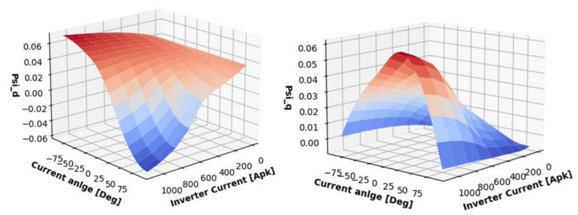

a) d-axis flux *b) q-axis flux*

Fig. 2. FEA results from the flux mapping at a field current of 18 A.

A small sensitivity study is reported in Table II, where the impact in terms of accuracy on the above-mentioned fundamental parameters can be noted by considering different resolutions of the electric cycle. The considered load point is characterized by a significant d-axis stator current, where the harmonic content in the flux is relatively high compared to other operating points of the motor. It is noted how only the torque ripple T_{ripple} effectively presents a significant difference by doubling the cycle resolution (about 5.28 %).

Concerning the settings of currents for the mapping, their amplitudes are extended beyond the expected operative limits of the motor to investigate other potential machine configurations by simply performing analytical scaling. This way, repeating the FEA mapping for each new machine configuration is avoided. Regarding the angle of the stator current vector, the first and second quadrants are fully explored by adopting a resolution of 5 electrical degrees. An example of the results from the FEA simulations is shown in Fig. 2, where the flux maps at a field current of 18 A are shown. It is noted how the domain of the flux maps is expressed in polar coordinates of the stator flux vector, i.e., each flux surface is plotted for a regular mesh grid of stator current amplitude and stator current angle.

B. Data Resolution

The FEA simulations executed to obtain the flux maps are very fast for a given field current value. However, depending on the adopted interpolation method, the levels of field current to consider to map the motor fully may be very high. It must be noted that the field current resolution is of significant importance. Indeed, a small variation of the field current can lead to a significant variation of the dq flux linkages for a given stator current vector. The proof of this is given in Fig. 3 and Fig. 4, where for a given speed, the stator voltage amplitude is plotted as a function of the field current and by considering two different operating points in terms of dq currents (I_d,I_q). The resolution of the field current is set at 0.5 A to avoid the wrong interpolation of flux and loss maps when implementing the MTPL algorithm.

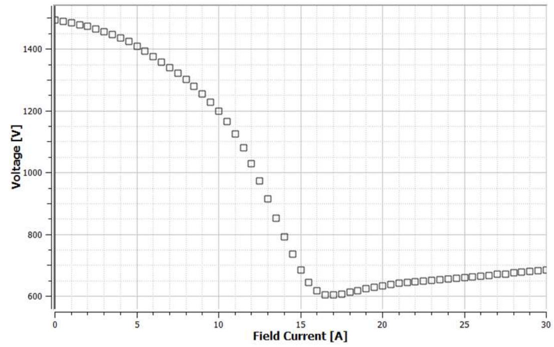

Fig. 3. Profile of the stator voltage amplitude at I_d = -375 A, I_q = 410 A.

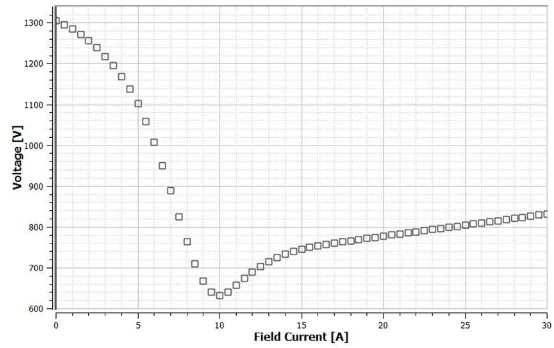

Fig. 4. Profile of the stator voltage amplitude at I_d = -260 A & I_q = 260 A.

V. IMPLEMENTATION OF MAXIMUM TORQUE PER LOSS

This Section presents the method used to solve the MTPL problem using an optimization algorithm in Python. Although this method is implemented to minimize the overall losses of the EESM, the same algorithm can be used to minimize any output parameter from the FEA simulations, such as field current, copper loss or torque ripple. However, in the case of minimizing torque ripple, a smaller step size is suggested in the FEA simulations to improve accuracy.

A. MTPL Algorithm

The algorithm to solve the MTPL problem is set up in two simple optimization steps. The first step consists in maximizing the torque at a given speed while applying constraints on the maximum currents and voltage. The torque produced by the EESM can be expressed analytically as a function of the current in the rotor and stator as

$$T(I_d, I_q, I_r) = \frac{3P}{2}\left(I_q \psi_d(I_d, I_q, I_r) - I_d \psi_q(I_d, I_q, I_r)\right) \quad (1)$$

where I_r is the field current while P denotes the number of rotor pole pairs, i.e., 4 pole pairs for the motor under consideration. About $\psi_d(I_d, I_q, I_r)$ and $\psi_q(I_d, I_q, I_r)$, these are interpolation functions of the *dq* flux maps obtained from the simulations described in the Section IV. In this study, a cubic interpolation method of the *dq* flux maps is used. The *dq* voltages U_d and U_q are calculated using the flux data and the voltage constrain can be set as:

$$U_d = R_{ph} I_d + \frac{d\psi_d(I_d, I_q, I_r)}{dt} - \omega_e \psi_q(I_d, I_q, I_r) \quad (2)$$

$$U_q = R_{ph} I_q + \frac{d\psi_q(I_d, I_q, I_r)}{dt} - \omega_e \psi_d(I_d, I_q, I_r) \quad (3)$$

$$U_{max} = \frac{U_{DC} \cdot MI}{\sqrt{3}} \geq \sqrt{U_d^2 + U_q^2} \quad (4)$$

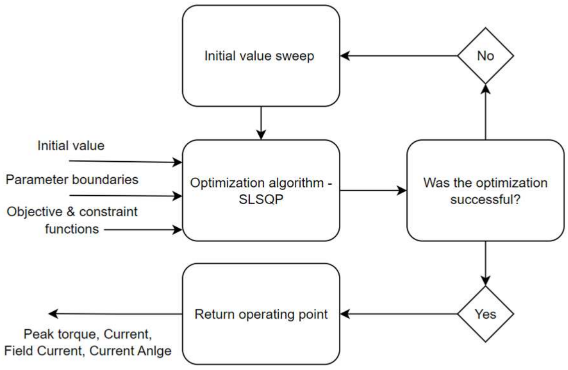

Fig. 5. Optimization method to obtain the peak torque.

where MI is the maximum modulation index of the inverter, ω_e is the rotor electrical speed, and R_{ph} is the stator phase resistance. The second constraint to be considered regards the motor currents since the limits of maximum inverter current I_{Rms} and maximum field current $I_{f,max}$ must not be exceeded, leading to as follows.

$$\sqrt{2} \cdot I_{Rms} \geq \sqrt{I_d^2 + I_q^2} \quad (5)$$

$$I_{f,max} \geq I_f \quad (6)$$

The first optimization can be set up by maximizing the torque equation (1) while fulfilling the constraints (4), (5) and (6). Python is used to perform the optimization, and the adopted optimization method is "Sequential Least Squares Programming". During the development of the mapping method, it has been noted that the optimization algorithm is sensitive to the initialization of the variables, making implementing a failure detection script necessary. Therefore, in the case of a failed optimization or unreasonable results, the three currents provided as input (i.e., I_d, I_q, and I_f) are appropriately changed to get the best result that is assumed as the final one. In Fig. 5, the optimization algorithm is represented using a block diagram to help understand it. Assuming sufficient data resolution from the flux mapping of the motor, this method is proved to be very robust.

As the peak torque is calculated, the second step of the optimization algorithm is performed, where the torque is stepped through from peak down to zero, and the losses are minimized for all speeds. In the FEA flux mapping, the losses are calculated individually, and the iron losses are divided up into iron losses in the stator yoke $P_{Fe_{Yoke}}$, in the stator teeth $P_{Fe_{Teeth}}$ and in the rotor lamination P_{Fe_Rotor}. For analysis purposes, separate interpolation functions are created for each loss component. Also, the raw data are corrected to account for the end-windings in the copper losses in the stator P_{Cu} and field winding and excitation system P_{Exc} The PWM effects on the iron losses are also accounted for in the calculation and is included as a correction factor into the weighting coefficients. The total losses P_{Loss} in the motor can thus be expressed as:

$$P_{Loss} = k_{Cu} P_{Cu}(I_d, I_q, I_r) + k_{Fe_{Yoke}} P_{Fe_{Yoke}}(I_d, I_q, I_r) + k_{Fe_{Teeth}} P_{Fe_{Teeth}}(I_d, I_q, I_r) + k_{Fe\_Rotor} P_{Fe\_Rotor}(I_d, I_q, I_r) + k_{Exc} P_{Exc}(I_d, I_q, I_r) \quad (7)$$

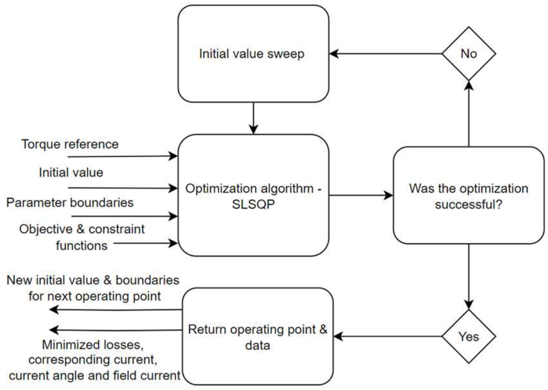

Fig. 6. MTPL optimization method.

where each loss component is associated with a weighting coefficient ($k_{Cu}, k_{Fe_{Yoke}}, k_{Fe_{Teeth}}, k_{Fe\_Rotor}, k_{Exc}$) which may be used to minimize a specific loss component in the MTPL optimization algorithm. In this study, all weights have been set unitary, which means that the total losses have been minimized, giving the most efficient solution for all operating points of the motor. In Fig. 6, the MTPL optimization algorithm is represented using a block diagram to help understand it. It is noted that optimal results found for an operating point are used to initialize the algorithm for the next operating point to be optimized. Moreover, the limits of stator and field currents, called 'boundaries' in Fig. 6, are updated according to the optimization results of the previous operating point. Indeed, for a given speed, the torque reference is decreased from an operating point to the subsequent one. Therefore, the amplitude stator and field currents must reduce from an operating point to the subsequent one as well, justifying the update of the boundaries in Fig. 6.

The algorithm is able to optimize around 17 operating points per minute using an Intel Core i7 processor with 8 cores and 16 logical processors. However, the computation time can be reduced significantly with a penalty on the accuracy, i.e., by decreasing the tolerance thresholds of the optimization algorithm.

VI. MTPL RESULTS

The MTPL optimization algorithm has been implemented to evaluate the optimal maps of current, flux and losses of the motor under consideration for a dc-link voltage of V_{dc} = 600 V. In Figs. 7 – 9, the optimal values of amplitude and angle of the stator current vector and field current are shown within the maximum torque per speed profile of the motor. It should be noted that the normalized current angle is relative to the *q*-axis meaning that negative values means operating in the first quadrant. In Fig. 10, the current, field current and current angle is plotted for constant torque operation with varying speed. It is noted that the active control of the field current allows the stator current vector to be kept close to the *q*-axis. Compared to a PMSM, it is thus noted that injecting a significant *d*-axis current component in the motor is unnecessary even in the flux-weakening region. Therefore, the EESM allows to significantly reduce the losses in the low-torque high/speed region.

The implemented MTPL algorithm aims to minimize the total losses of the EESM, thereby obtaining the loss maps shown in Figs. 11 – 13. The complete efficiency map of the studied machine is shown in Fig. 16.

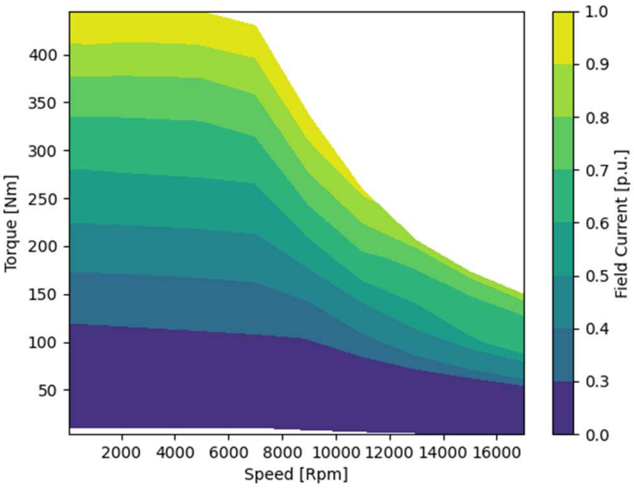

Fig. 7. Field current map of the EESM at V_{dc} = 600 V.

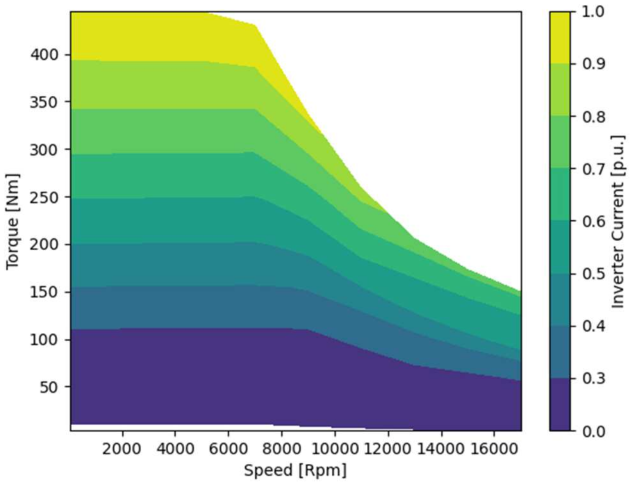

Fig. 8. Stator current amplitude map of the EESM at V_{dc} = 600 V.

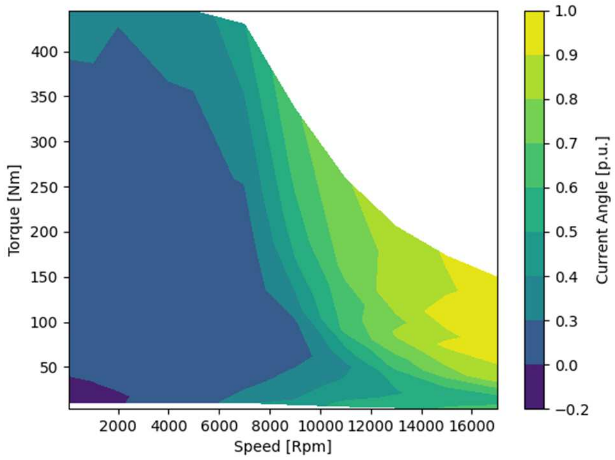

Fig. 9. Stator current angle map of the EESM at V_{dc} = 600 V.

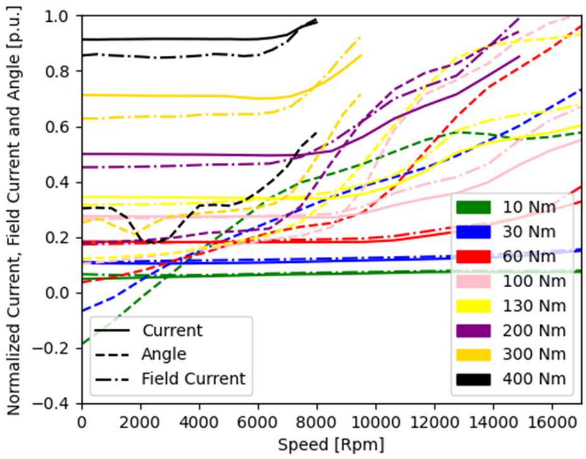

Fig. 10. Current angle and field current plotted against speed for constant torque operation.

It should be noted that each loss component is reported in terms of the percentage of the total loss at each operating point for Figs. 11 – 13. The overall loss breakdown may vary depending on the specific machine design and how the overall losses are distributed within the machine.

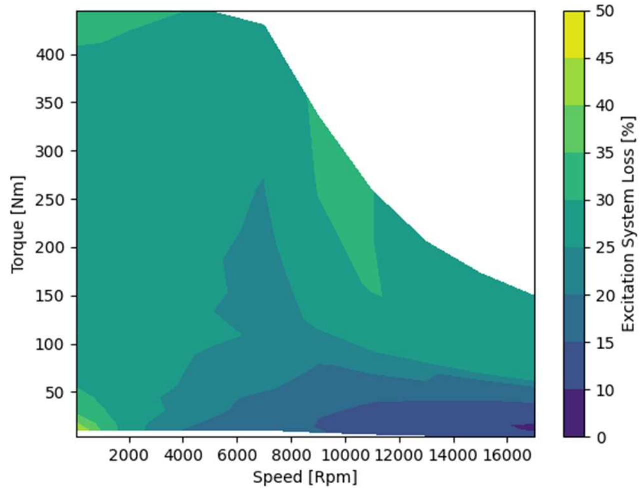

Fig. 11. Excitation system losses map of the EESM at V_{dc} = 600 V.

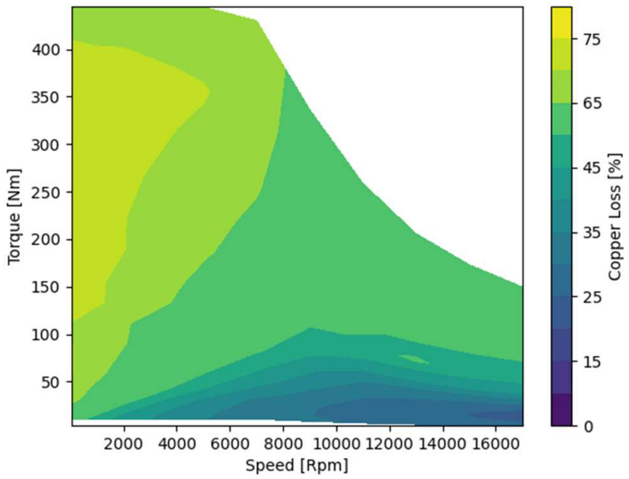

Fig. 12. Copper losses map of the EESM at V_{dc} = 600 V.

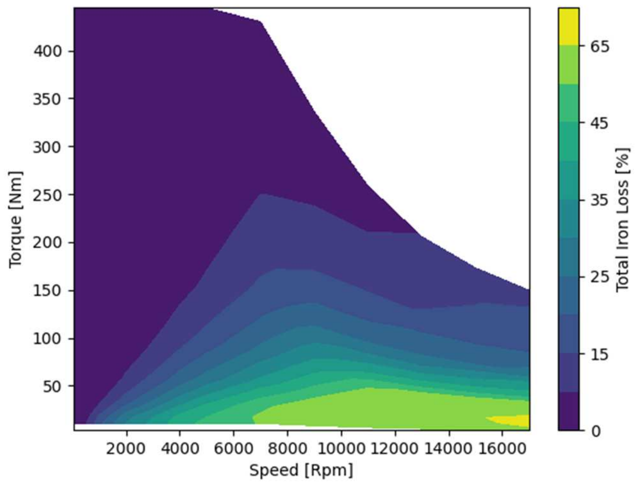

Fig. 13. Iron losses map of the EESM at V_{dc} = 600 V.

In Fig. 14 and Fig. 15, the maps of the *dq* flux linkages are shown where it is noted that the *d*-axis flux is high for most of the constant torque region in which the motor is operating in the field-strengthening region.

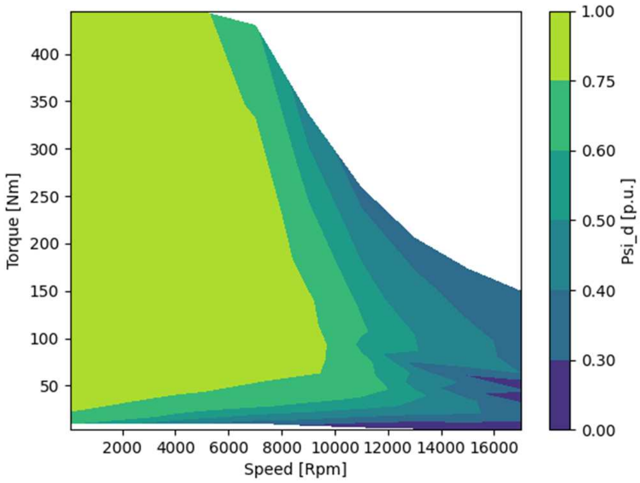

Fig. 14. D-axis flux linkage map of the EESM at V_{dc} = 600 V.

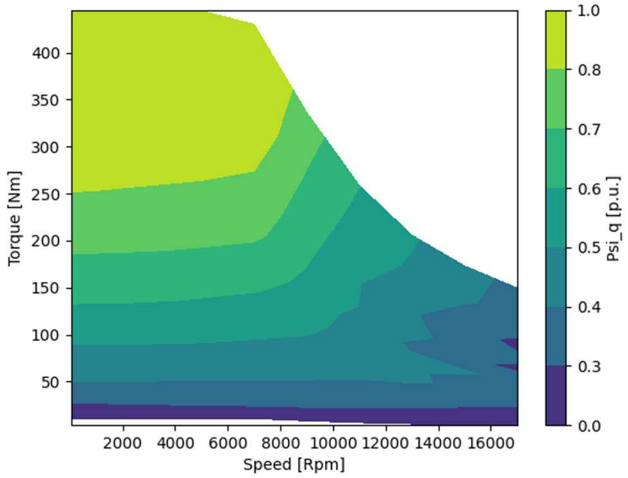

Fig. 15. Q-axis flux linkage map of the EESM at V_{dc} = 600 V.

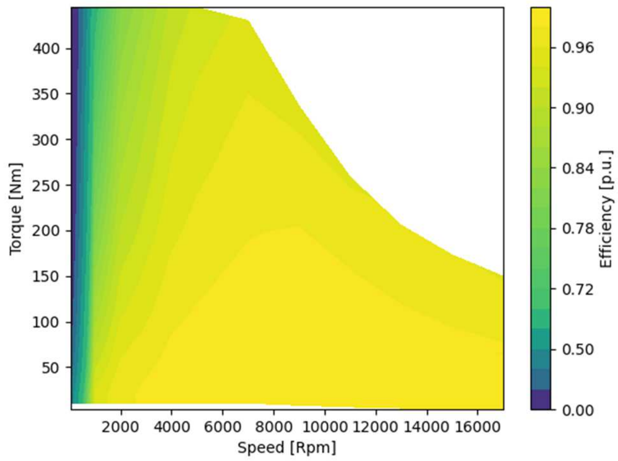

Fig. 16. Efficiency map of the EESM at V_{dc} = 600 V.

VII. Conclusions

In this paper, a methodology to obtain the performance and efficiency maps of electrically excited synchronous machines (EESM) has been presented. The method is based on minimizing the losses for a given torque (MTPL) based on data from FEA simulations. This way, the efficiency map, as well as the optimal operating conditions at each operating point, can be computed. In addition, the method can easily be adapted to minimize copper losses, which may be practically more straightforward to implement on an electric drive.

Future improvements to the algorithm can be performed such that losses are minimized for the entire electric drive rather than just the motor losses. This can be achieved by including losses of power electronics converters used to feed the rotor and stator windings. The Improvements could be implemented separately, or together, with an experimental verification of the method.

ACKNOWLEDGMENT

The authors would like to thank Polestar Performance AB for financing this research and providing software licenses and computing hardware to develop the described method. The authors would also like to thank the Polestar Electric Drive Unit – EMD & CAE team for their contributions in development of the studied machine.

REFERENCES

[1] A. Krings and C. Monissen, "Review and Trends in Electric Traction Motors for Battery Electric and Hybrid Vehicles," 2020 International Conference on Electrical Machines (ICEM), Gothenburg, Sweden, 2020, pp. 1807-1813, doi: 10.1109/ICEM49940.2020.9270946.

[2] E. Carraro, M. Degano and N. Bianchi, "Permanent magnet volume minimization in permanent magnet assisted synchronous reluctance motors," 2013 Eighth International Conference and Exhibition on Ecological Vehicles and Renewable Energies (EVER), Monte Carlo, Monaco, 2013, pp. 1-4, doi: 10.1109/EVER.2013.6521539.

[3] B. Raghuraman, S. Nategh, N. Sidiropoulos, L. Petersson and A. Boglietti, "Sustainability Aspects of Electrical Machines For E-Mobility Applications Part I: A Design with Reduced Rare-earth Elements," IECON 2021 – 47th Annual Conference of the IEEE Industrial Electronics Society, Toronto, ON, Canada, 2021, pp. 1-6, doi: 10.1109/IECON48115.2021.9589246.

[4] Z. Yang, F. Shang, I. P. Brown and M. Krishnamurthy, "Comparative Study of Interior Permanent Magnet, Induction, and Switched Reluctance Motor Drives for EV and HEV Applications," in IEEE Transactions on Transportation Electrification, vol. 1, no. 3, pp. 245-254, Oct. 2015, doi: 10.1109/TTE.2015.2470092.

[5] G. Petrelli, S. Nuzzo, T. Zou, D. Barater, G. Franceschini and C. Gerada, "Review and Future Developments of Wound Field Synchronous Motors in Automotive," 2023 IEEE International Conference on Electrical Systems for Aircraft, Railway, Ship Propulsion and Road Vehicles & International Transportation Electrification Conference (ESARS-ITEC), Venice, Italy, 2023, pp. 1-6, doi: 10.1109/ESARS-ITEC57127.2023.10114826.

[6] J. Tang, "Design and Control of Electrically Excited Synchronous Machines for Vehicle Applications," Doctoral Thesis, Chalmers University of Technology, 2021.

[7] G. Mademlis, Y. Liu, J. Tang, L. Boscaglia and N. Sharma, "Performance Evaluation of Electrically Excited Synchronous Machine compared to PMSM for High-Power Traction Drives," 2020 International Conference on Electrical Machines (ICEM), Gothenburg, Sweden, 2020, pp. 1793-1799, doi: 10.1109/ICEM49940.2020.9270852.

[8] T. M. Jahns and V. Caliskan, "Uncontrolled generator operation of interior PM synchronous machines following high-speed inverter shutdown," in IEEE Transactions on Industry Applications, vol. 35, no. 6, pp. 1347-1357, Nov.-Dec. 1999, doi: 10.1109/28.806049.

[9] M. G. Pasquinelli, P. Bolognesi, A. Guiducci, S. Nuzzo and M. Galea, "Design of a High-Speed Wound-Field Synchronous Generator for the More Electric Aircraft," 2021 IEEE Workshop on Electrical Machines Design, Control and Diagnosis (WEMDCD), Modena, Italy, 2021, pp. 64-69, doi: 10.1109/WEMDCD51469.2021.9425625.

[10] A. Mahmoudi, W. L. Soong, G. Pellegrino, E. Armando, "Efficiency maps of electrical machines", Conf. Rec. ECCE, pp. 2791-2799, 2015.